

## ANALYSIS OF OPTICAL SPECTROSCOPY AND PHOTOMETRY OF THE TYPE I X-RAY BURSTING SYSTEM UW CRB

M. R. KENNEDY<sup>1,2</sup>, P. CALLANAN<sup>1</sup>, P. M. GARNAVICH<sup>3</sup>, R. P. BRETON<sup>2</sup>, A. J. BROWN<sup>4</sup>, N. CASTRO SEGURA<sup>5</sup>, V. S. DHILLON<sup>6,7</sup>, M. J. DYER<sup>6</sup>, S. FIJMA<sup>8</sup>, J. GARBUTT<sup>6</sup>, M. J. GREEN<sup>9</sup>, P. HAKALA<sup>10</sup>, F. JIMINEZ-IBARRA<sup>11</sup>, P. KERRY<sup>6</sup>, S. LITTLEFAIR<sup>6</sup>, J. MUNDAY<sup>5</sup>, P. A. MASON<sup>12,13</sup>, D. MATA-SANCHEZ<sup>7,14</sup>, T. MUNOZ-DARIAS<sup>7,14</sup>, S. PARSONS<sup>6</sup>, I. PELISOLI<sup>5</sup>, D. SAHMAN<sup>6</sup>

<sup>1</sup>Department of Physics, University College Cork, Cork, Ireland

<sup>2</sup>Jodrell Bank Centre for Astrophysics, School of Physics and Astronomy, The University of Manchester, M13 9PL, UK

<sup>3</sup>Department of Physics, University of Notre Dame, Notre Dame, IN, USA

<sup>4</sup>Departament de Física, Universitat Politècnica de Catalunya, c/Esteve Terrades 5, 08860 Castelldefels, Spain

<sup>5</sup>Department of Physics, University of Warwick, Coventry CV4 7AL, UK

<sup>6</sup>Department of Physics and Astronomy, University of Sheffield, Sheffield S3 7RH, UK

<sup>7</sup>Instituto de Astrofísica de Canarias, E-38205 La Laguna, Tenerife, Spain

<sup>8</sup>Anton Pannekoek Institute for Astronomy, University of Amsterdam, Science Park 904, NL-1098 XH Amsterdam, the Netherlands

<sup>9</sup>Max-Planck-Institut für Astronomie, Königstuhl 17, D-69117 Heidelberg, Germany

<sup>10</sup>Finnish Centre for Astronomy with ESO (FINCA), Quantum, University of Turku, FI-20014, Finland

<sup>11</sup>School of Physics and Astronomy, Monash University, Clayton Campus, VIC 3800, Australia

<sup>12</sup>New Mexico State University, MSC 3DA, Las Cruces, NM 88003, USA

<sup>13</sup>Picture Rocks Observatory, 1025 S. Solano Dr. Suite D., Las Cruces, NM 88001, USA and

<sup>14</sup>Departamento de Astrofísica, Univ. de La Laguna, E-38206 La Laguna, Tenerife, Spain

Version August 14, 2024

### ABSTRACT

UW Coronae Borealis (UW CrB) is a low mass X-ray binary that shows both Type 1 X-ray and optical bursts, which typically last for 20 s. The system has a binary period of close to 2 hours and is thought to have a relatively high inclination due to the presence of an eclipse in the optical light curve. There is also evidence that an asymmetric disc is present in the system, which precesses every 5.5 days based on changes in the depth of the eclipse. In this paper, we present optical photometry and spectroscopy of UW CrB taken over 2 years. We update the orbital ephemeris using observed optical eclipses and refine the orbital period to 110.97680(1) min. A total of 17 new optical bursts are presented, with 10 of these bursts being resolved temporally. The average  $e$ -folding time of  $19 \pm 3$  s for the bursts is consistent with the previously found value. Optical bursts are observed during a previously identified gap in orbital phase centred on  $\phi = 0.967$ , meaning the reprocessing site is not eclipsed as previously thought. Finally, we find that the apparent P-Cygni profiles present in some of the atomic lines in the optical spectra are due to transient absorption.

### 1. INTRODUCTION

UW Coronae Borealis (UW CrB), also known as MS 1603.6+2600, was discovered by the *Einstein Observatory* Extended Medium Sensitivity Survey as an unusual binary with an orbital period of close to 2 hours (Morris et al. 1990). It was unusual in that it did not match the properties of any known cataclysmic variable (an interacting binary with a white dwarf primary; CV) and no Low Mass X-ray Binary (LMXB) had been discovered which had an orbital period in the 1-2 hour range. The optical spectrum of the source showed a strong blue continuum, Balmer, HeI, and HeII emission lines, and the Bowen blend emission feature at 4640 Å, and optical light curve showed variations on a timescale of 2 hours (hence the orbital period estimate). However, the general shape and orbital phase of these variations were found to change from night to night. Hakala et al. (1998) confirmed the variations in the optical light curve, and also ruled out a non-magnetic CV classification for UW CrB. They preferred an LMXB classification for UW CrB, despite its short orbital period. Mukai et al. (2001) finally confirmed UW CrB as a LMXB with a neutron star (NS) primary after the discovery of a type I X-ray burst in the X-ray light curve obtained using the *Advanced Satellite for Cosmology and Astrophysics* (ASCA).

Type I X-ray bursts are indicative of a NS primary as they are thought to arise during brief periods of thermonuclear runaway on the surface of the NS. Type I X-ray bursts are typically short in duration, with a sharp rise lasting between 1 – 10 s and slow decay lasting between 10 s and a few minutes (see Parikh et al. 2013 for a review). The observed bursts in UW CrB match this description perfectly, with rise times of  $< 5$  s and a decay time of  $\sim 20$  s.

However, it is not just these X-ray bursts that make UW CrB an interesting system. Hynes et al. (2004) and Muhli et al. (2004) discovered that UW CrB also produces optical bursts that last between 15–30 s and increase the optical flux from the system by a factor of 2–3. They proposed that these optical bursts are counterparts to the X-ray bursts, and are produced by reprocessing of the X-ray bursts by material in the system. These type I optical bursts are not unique to UW CrB, and have been seen in a handful of other systems (MXB 1735-44, Grindlay et al. 1978; V801 Arae and UY Volantis, Schoembs & Zoeschinger 1990; Aquila X-1, Robinson & Young 1997; GS 1826-24, Homer et al. 1998; and others). Determination of the exact correlation between the optical and X-ray bursts seen in UW CrB has been hampered by the lack of any simultaneous X-ray and optical observations.

Since 2004, multiple optical observations of UW CrB have revealed more about the nature of the binary. [Mason et al. \(2008\)](#) refined the orbital period to 110.97671 min, and discovered that the nightly variations in the shape and width of the eclipse varied periodically with a 5.5 day period. They proposed that such behaviour can be explained by an asymmetric accretion disc in the system which precesses around the NS once every 5.5 days. [Hakala et al. \(2009\)](#) confirmed the super-orbital period of 5.5 days, and also analysed 11 more optical bursts, finding a similar duration to [Hynes et al. \(2004\)](#). [Mason et al. \(2012\)](#) presented analysis of an additional 9 optical bursts, and combined the optical bursts from their work with the bursts presented in [Hynes et al. \(2004\)](#) and [Hakala et al. \(2009\)](#). They found that no optical bursts had been observed during an orbital phase gap centred on orbital phase 0.967 and with a width of  $\delta\phi = 0.210$ , and suggested that this was due to an eclipse of the reprocessing site by the companion star. Here, and in the rest of this paper, an orbital phase of zero occurs when the companion star is at inferior conjunction. Finally, and most recently, [Fijma et al. \(2023\)](#) presented ultraviolet spectra of UW CrB taken with the Cosmic Origins Spectrograph onboard the Hubble Space Telescope in 2011. In these data, a transient P Cygni profile, indicative of an outflow, is visible. These authors consider in detail whether a disc wind would be expected in a system with parameters consistent with UW CrB, while also mentioning that such line profiles could also arise from irradiation driven evaporation of the companion star, or an outflow coming from the interaction point (the “hot spot”) between the ballistic stream and the accretion disc.

Here, we present new optical photometry taken with the intent to extend the optical ephemeris from [Mason et al. \(2012\)](#), and also to observe and characterise more optical bursts. We also present optical spectroscopy of UW CrB, the first taken in 20 years.

## 2. OBSERVATIONS

Below, we detail observations taken of UW CrB between 2014 and 2019.

### 2.1. VATT & LBT Photometry

Optical photometry observations of UW CrB were carried out over 10 nights between 2014-2016. Table 1 shows the full details of individual observations. The Vatican Advanced Technology Telescope (VATT) 2014 observations were taken using the VATT4K CCD with a 20 s exposure time and additional 14 s overhead, and with a SDSS- $g'$  filter inserted. The Large Binocular Telescope (LBT) 2014 observations were taken using the Large Binocular Camera (LBC, [Giallongo et al. 2008](#)) mounted on the DX (right side) of the telescope with a Johnson V filter inserted. The VATT 2015 and 2016 observations were taken using the Galway Ultrafast Imager (GUFU, [Harding et al. 2013](#)) with varying exposure times, without any filter so as to increase the S/N of the detection of the source in each frame. The advantage of using GUFU over the VATT4K is that GUFU is a frame transfer CCD and has negligible read out time. The data were bias corrected and flat fielded using IRAF<sup>1</sup>, and simple aper-

TABLE 1  
DETAILS OF THE VARIOUS OPTICAL OBSERVATIONS OF UW CrB  
BETWEEN 2014 AND 2019.

Date (UT)	Instrument	Cadence (s)	No. of Frames	Phase Coverage
2014-04-29	VATT4K	34	335	0.3-2.3
2014-04-30	VATT4K	34	212	0.3-1.1
2014-04-02	VATT4K	34	166	0.9-1.7
2014-06-30	VATT4K	34	270	0.1-1.4
2014-06-30	LBC	34	169	0.6-1.5
2014-07-01	VATT4K	34	366	0.5-2.3
2015-04-10	GUFU	15	1130	0.2-2.9
2015-04-11	GUFU	15	1151	0.2-2.8
2016-06-03	GUFU	10	1020	0.5-2.1
2016-06-04	GUFU	10	1387	0.0-2.2
2016-06-07	GUFU	17	583	0.4-1.8
2019-07-08	HiPERCAM	0.5	30101	0.0-1.75

ture photometry with one comparison star was used to extract the light curve. Figure 1 shows the light curve from each individual run.

### 2.2. LBT Spectroscopy

While LBC on the DX mirror of the LBT was taking photometry of UW CrB, the Multi-Object Dual Spectrographs (MODS1; [Pogge et al. 2010](#)) on the SX mirror (left side) was taking simultaneous spectroscopy of UW CrB. MODS1 in the dual grating mode covers a wavelength range from 320 nm to 1  $\mu\text{m}$ , divided into red and blue channels separated by a dichroic at 560 nm. The exposure for each spectrum was 60 s and the time between the start of consecutive exposures averaged 120 s. The readout time of the red channel on the MODS instrument is faster than on the blue channel, meaning the red set of spectra finished before the blue set, leading to a slightly different time coverage in the separate channels. Fifty spectra were obtained from each channel between 06:18 UT and 7:54 UT. The data reduction tasks were carried out using IRAF.

### 2.3. HiPERCAM Photometry

UW CrB was observed using the quintuple beam photometer HiPERCAM ([Dhillon et al. 2021](#)) mounted on the 10.8m Gran Telescopio Canarias, starting at 2019-07-08 23:00:37 and lasting for 2 hours and 20 minutes. HiPERCAM provides five simultaneous bands of optical photometry with a readout time  $\sim 6$  ms. The data were acquired with Super-SDSS  $u_s$ ,  $g_s$ ,  $r_s$ ,  $i_s$  and  $z_s$  filters, which are filters that cover the same wavelength range as the traditional SDSS  $u'$ ,  $g'$ ,  $r'$ ,  $i'$ , and  $z'$  filters ([Doi et al. 2010](#)), but with a higher throughput ([Dhillon et al. 2021](#)). The exposure time for each frame was 0.5 s. The data were reduced using the purpose-built HiPERCAM pipeline (as described in [Dhillon et al. 2021](#)) using biases and flat field observations from that same night. The light curve of these observations are presented on their own in Figure 2, along with the ratio of fluxes of each band relative to the  $g_s$ . This is provided to demonstrate that the colour of the system does not vary significantly over the orbital period.

<sup>1</sup> IRAF is distributed by the National Optical Astronomy Observatories, which are operated by the Association of Universities

for Research in Astronomy, Inc., under cooperative agreement with the National Science Foundation.

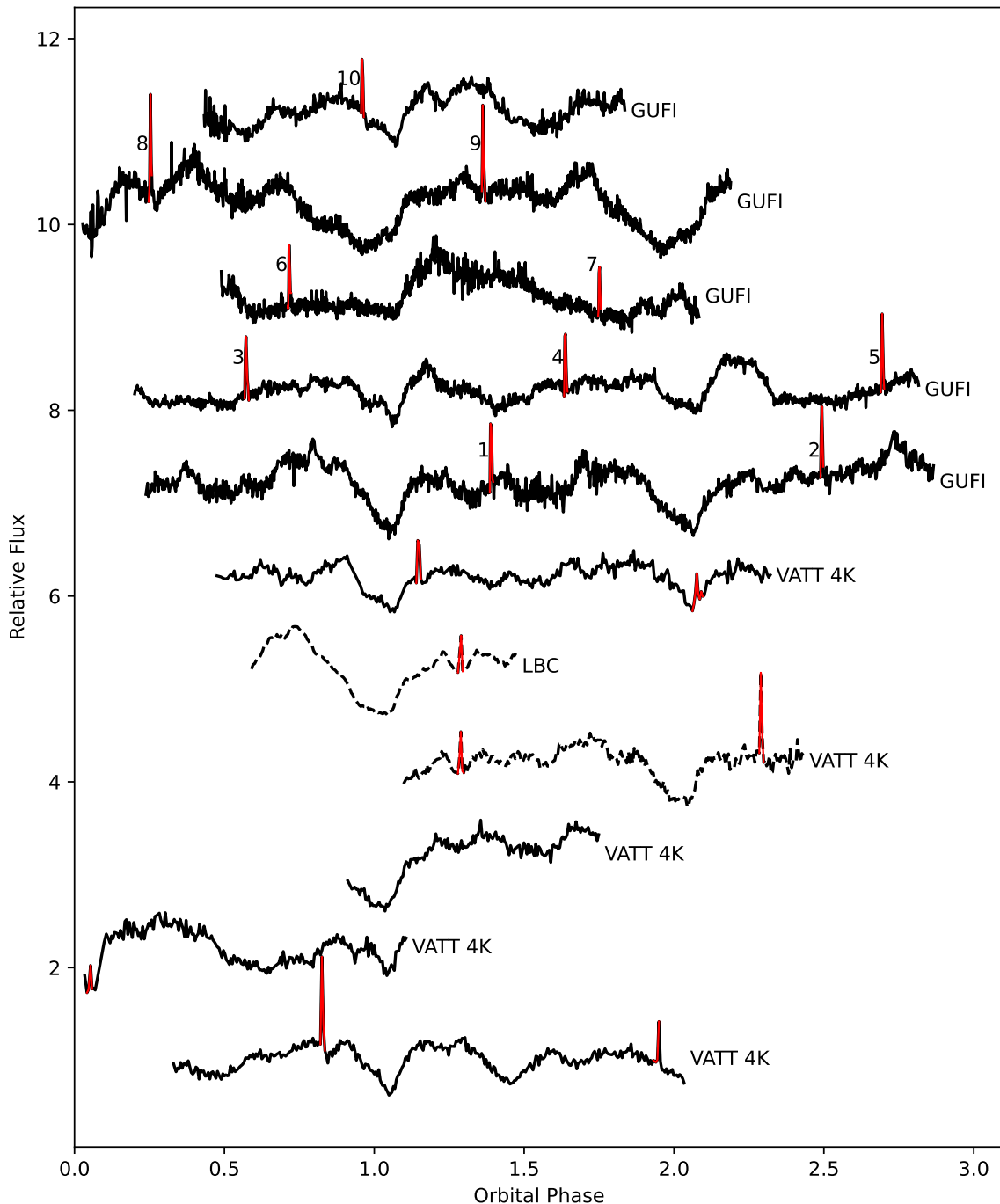


FIG. 1.— The individual light curves for each observation listed in Table 1. The light curves have been offset from each other by a constant factor, and are plotted in ascending order, with the bottom light curve taken on 2014-04-29 and the top light curve taken on 2016-06-07. The data plotted in red are optical bursts whose identification is described in the text. The 10 bursts taken using the GUF1 instrument, which are numbered 1-10, are analysed in depth in Section 3.3. Note that the data taken on 2014-06-30 from the VATT and LBT (shown as dashed black lines) overlap, and show the same bursts.

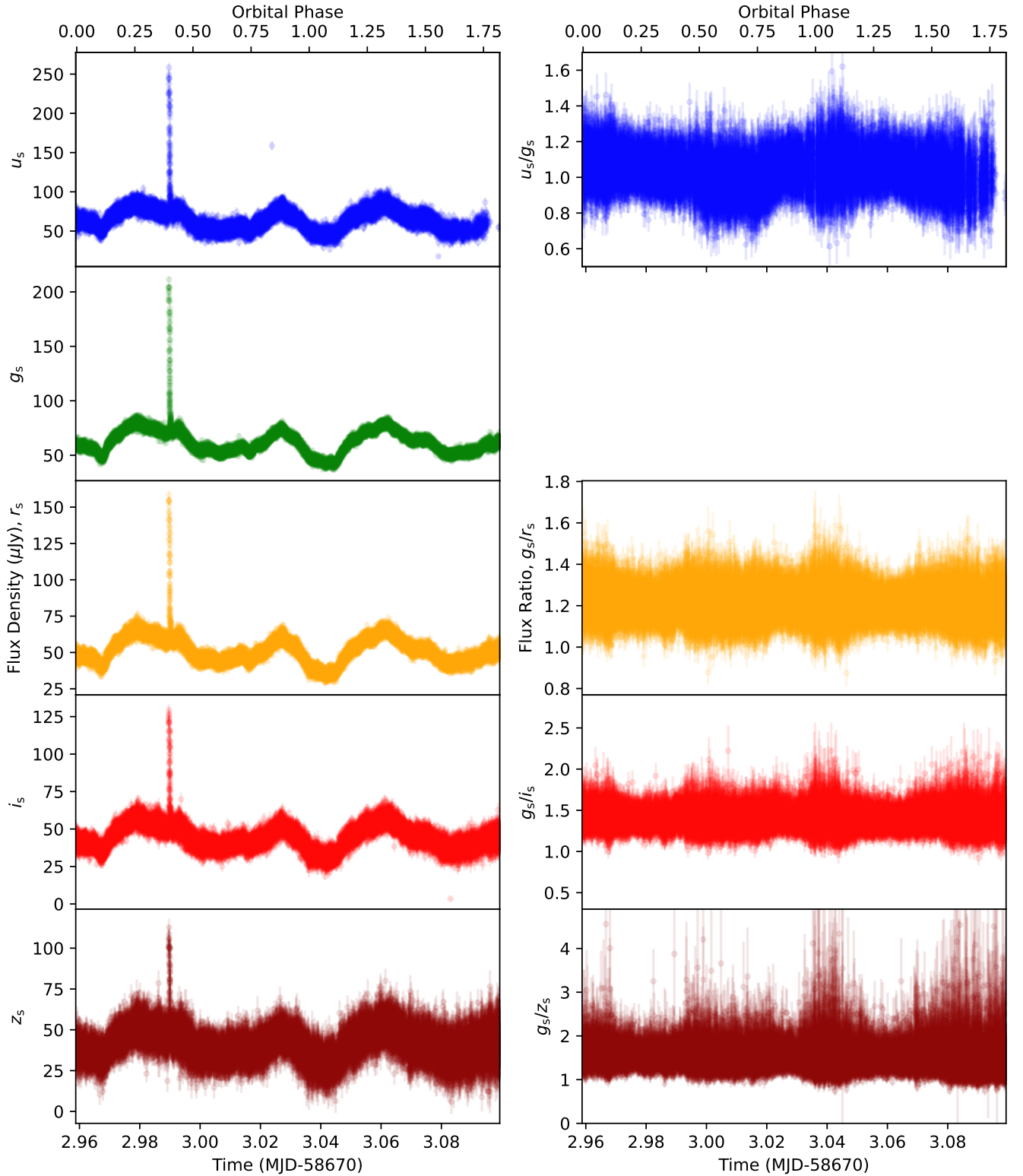


FIG. 2.— HiPERCAM light curve of UWCRB. *Left column:* Each panel represents a different filter, with  $u_s$  on top and  $z_s$  on bottom. There is a single burst detected in all filters. The time resolution of this light curve is 0.5 s, a substantial increase on the data shown in Figure 1. The orbital phase of the binary is given as the top axis, and was calculated using the ephemeris presented in this paper. *Right column:* The ratio of fluxes in each band. The top panel shows the  $u_s$  flux relative to the  $g_s$  flux, while the other panels show the  $g_s$  flux relative to the corresponding band in the left column. This is included to show the small variation in the colour of the system over an orbital period.

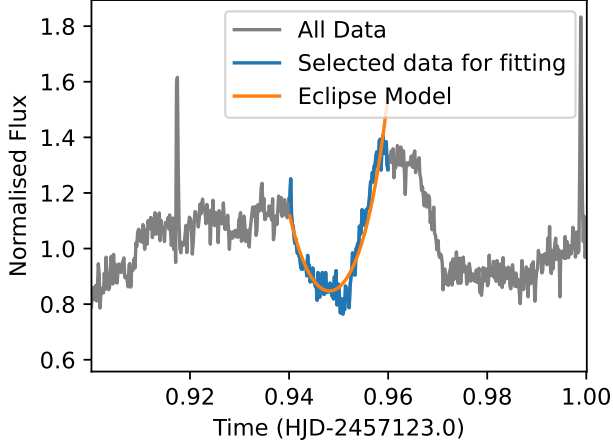


FIG. 3.— An example of the quadratic fit to eclipse data. The grey line shows the normalised flux, while the highlighted blue data are those that were selected as the eclipse data. The orange line shows the quadratic fit to these data.

#### 2.4. Hubble Space Telescope Cosmic Origins Spectrograph data

We additionally include three epochs of data taken of UW CrB using the Cosmic Origins Spectrograph (COS, Green et al. 2012) on the Hubble Space Telescope (HST). Epoch one covered 02:15 to 09:12 UT on September 1, 2011, and was first presented in Fijma et al. (2023). Epoch two covered several windows between August 21 and August 22 2023. Epoch three covered 18:04 UT to 20:18 UT on February 21, 2024. Detailed analysis of the second and third epochs are on going, but here we include the timing of the bursts observed in these data when discussing the phases at which optical bursts from UW CrB are observed. While each epoch were taken using HST/COS, the 2011 data, in which an optical burst is present, were obtained using the G160M grating (spanning  $\sim 1360$ - $1775$  Å), and the 2023 and 2024 data were obtained using the G140L grating (spanning  $\sim 1100$ - $2290$  Å). Light curves were generated using data taken within a wavelength range of  $1415$ - $1770$  Å for the former and  $1170$ - $2000$  Å for the latter. Here the geocoronal Lyman- $\alpha$  ( $1208$ - $1225$  Å) and O I ( $1298$  to  $1312$  Å) line profiles were masked, as well as low signal-to-noise regions near the edges of the gratings

### 3. RESULTS

#### 3.1. Orbital Ephemeris

The data presented fully sampled 13 eclipses and partially sampled 3 eclipses. Table 2 lists the mid times of these eclipses. Since the eclipse changes profile not only from night to night, but also from orbit to orbit, it is impossible to pick a single feature in the eclipse that could serve as a reference point for calculating the mid-eclipse time. As such, we identified the eclipse ingress and egress in each light curve, fit a quadratic function to the data spanning this range, and set the eclipse mid-time to the centre of this quadratic fit. An example of this is shown in Figure 3.

The corresponding eclipse numbers were calculated using the orbital ephemeris presented in Mason et al. (2012). These eclipse times were added to the 32 mid-

TABLE 2  
MID-ECLIPSE TIMES FOR THE 16 ECLIPSES IN THE NEW DATA.

Eclipse No.	Mid-eclipse Time (HJD)	Error (day)
47465	2456776.8384	0.0007
47477	2456777.764	0.001
47505	2456779.9180	0.0007
48269	2456838.7972	0.0007
48270	2456838.8746	0.0007
48282	2456839.8008	0.0007
48283	2456839.880	0.001
51955	2457122.8696	0.0007
51956	2457122.9465	0.0007
51968	2457123.8728	0.0007
51969	2457123.9481	0.0007
57403	2457542.728	0.001
57415	2457543.655	0.001
57416	2457543.7286	0.0007
57417	2457543.8042	0.0007
57455	2457546.7397	0.0007

eclipse times from Mason et al. (2012) and the 24 mid-eclipse times from Mason et al. (2008). All 72 mid-eclipse times were fit to determine an accurate ephemeris. The resulting linear ephemeris was

$$T_{mid}(HJD) = 2453118.8390(4) + 0.077067223(9)E. \quad (1)$$

The O-C curve for this linear ephemeris is shown in Figure 4, and this ephemeris was used for calculating the orbital phases shown in Figure 1. The  $\chi^2$  value for this fit was 1388 for 70 degrees of freedom. A quadratic fit to the mid-eclipse times was also tested, which gave a quadratic ephemeris of

$$T_{mid}(HJD) = 2453118.8377(4) + 0.077067235(9)E + (8(2) \times 10^{-13})E^2. \quad (2)$$

The  $\chi^2$  value for this fit was 1213 for 69 degrees of freedom. While the quadratic ephemeris provides an improvement in  $\chi^2$ , there is still significant scatter in the O-C constructed using this ephemeris. This is most likely related to the known variation in the mid-eclipse time across the 5.5 day period which has been attributed to a precessing accretion disc in the system. Without knowledge of the disc phase during our observations (none of our observations cover a continuous 5.5 days), it is impossible to tell if the additional term in the quadratic ephemeris is due to a change in the orbital period, or just related to minimising this scatter. Performing an F-test using the variances of the residuals of both ephemerides gives a P value of 0.22, which suggests we cannot reject with high confidence the null-hypothesis that the linear model is a good fit to the data, and given that the orbital period in both ephemerides agree within  $1\sigma$ , we adopt the linear ephemeris for the rest of this paper.

#### 3.2. Optical Spectrum

The average optical spectrum is shown in Figure 5. The most prominent emission and absorption lines are marked, which correspond to H $\alpha$ , H $\beta$ , a series of HeI and HeII lines, and the Bowen blend structure (CIII and NIII) at  $4640$  Å. The most interesting features of the optical spectrum are the absorption features seen in the



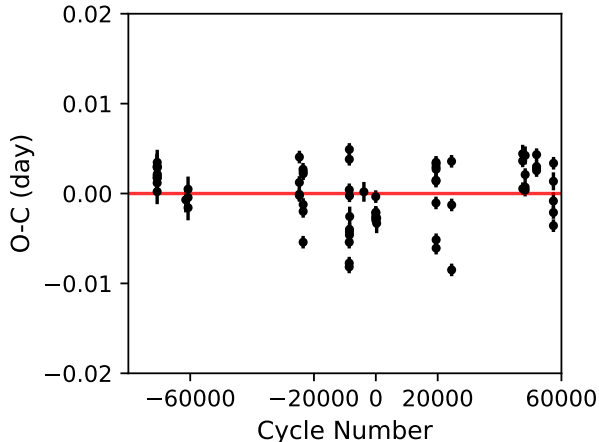


FIG. 4.— The observed-calculated times of mid-eclipse for UW CrB. The cycle number was calculated using Equation 1.

HeI lines and in  $H\beta$ . Figure 6 shows the time averaged line profile of HeI 5875 Å alongside  $H\beta$ . The average line profiles resemble a P Cygni line profile, which are characterised by blue-shifted absorption components and a red-shifted emission component. Such line profiles, first proposed by Beals (1929), are indicative of an outflow of material from a system and have been studied in detail in the context of LMXBs and CVs. They often vary in strength (e.g., depending on the flaring activity during the outburst), can be transient in nature (vanishing over shorter than hourly timescales), and can be difficult to interpret (see for example Muñoz-Darias et al. 2016 and Muñoz-Darias et al. 2019).

To understand the line profile better, trailed spectra for  $H\alpha$ ,  $H\beta$ , HeI 5875 Å, and HeII 4686 Å are given in Figure 7. These plots highlight the transient nature of the absorption feature in several of these lines. From the  $H\alpha$  plot, we can see that the emission peak is largely confined to positive velocities. HeII, on the other hand, shows clear blue and red emission components both before and after eclipse. HeI shows absorption at negative velocities prior to the eclipse, and very little absorption or emission after the eclipse.

Figure 8 shows the normalised trailed spectrum around HeI 5875 Å. When compared to Figure 2 of Muñoz-Darias et al. 2016, which shows the standard behaviour for P Cygni profiles in LMXBs where both emission and absorption components are visible simultaneously, it becomes apparent that the behaviour of the line profile of HeI in the spectrum of UW CrB is not that of a conventional P Cygni line, where the absorption component is visible without any emission counterpart for orbital phase 0.6–0.93. Then, around the time of optical eclipse, the line undergoes a reversal, with the absorption feature becoming weaker, and a strong, red-shifted emission component develops in the line profile. Finally, at orbital phase 0.16, both features disappear (or, at the very least, become significantly weaker, as shown by the top average spectrum shown in Figure 8). The strong emission seen around orbital phase 0 is probably due to a weakening of the continuum as the accretion disc is eclipsed, allowing for the line to become detectable, as opposed to an actual strengthening of the emission line itself. This sug-

gests that the emission feature is present for the whole orbit and, outside of eclipse, it is drowned out by the continuum. Thus, we only treat the absorption feature as transient.

### 3.2.1. Optical Burst Spectrum

The top panel of Figure 9 shows the LBC light curve around the time of the optical burst seen in the LBT data. Fortunately, both the blue and red sides of the spectrograph were exposed when this burst occurred. This observed spectrum is shown in the main panel of Figure 9, and has a stronger continuum than the spectra taken before and after the burst. However, no changes in any of the emission lines is detectable, with  $H\alpha$  being the best resolved emission feature. The residual spectrum (burst spectrum - average spectrum) is consistent with having a spectral index of 0 (that is, the spectrum is flat). This means we cannot get any temperature constraints on the burst from the optical spectrum. The detection of the optical burst spectrum is promising, and suggests a larger telescope will be able to obtain higher signal-to-noise burst spectra which will help constrain the site of the optical reprocessing. The physical origin of the feature around 7700 Å in the optical burst spectrum is unknown, but is visible in several spectra throughout the orbit, suggesting it is not related to the burst.

### 3.3. Optical Bursts

A total of 18 optical bursts were detected in all of the observations taken of UW CrB - 17 with using the VATT, 1 using the LBT, and 1 using the GTC. For the VATT and LBT data, these bursts were identified in the observed light curves by looking for points which were more than  $3\sigma$  away from the median of the surrounding 40 points, where  $\sigma$  is the standard deviation of the 40 points. These bursts were then inspected by eye as a final confirmation step. Seven of these bursts were detected using the VATT4K instrument with a temporal resolution of 35s, one of which was also detected in the LBC observations. Since the optical bursts have been observed to have an  $e$ -folding time of 20s, this means the VATT4K observations were unable to resolve bursts, with each burst only recorded as a single data point in the light curves. Even though the structure of these bursts cannot be explored, the orbital phases at which they were detected is important, and will be discussed in Section 3.3.3.

#### 3.3.1. Modelling the optical bursts I - GUF1

There were ten bursts detected using the GUF1 instrument with a temporal resolution of 15s or better. These bursts were fit using an instantaneous rise and exponential decay model, as done previously by Hynes et al. (2004) and Hakala et al. (2009), after subtraction of a linear fit to the data around the burst to account for the orbital variation in the light curve. This model has the form

$$F(t) = A e^{\left(\frac{t-t_0}{\tau}\right)}, \quad (3)$$

where  $A$  is the peak amplitude of the burst,  $t_0$  is the start time of the burst, and  $\tau$  is the  $e$ -folding time of the bursts. The fitting was performed using MULTINEST (Feroz & Hobson 2008; Feroz et al. 2009; Feroz

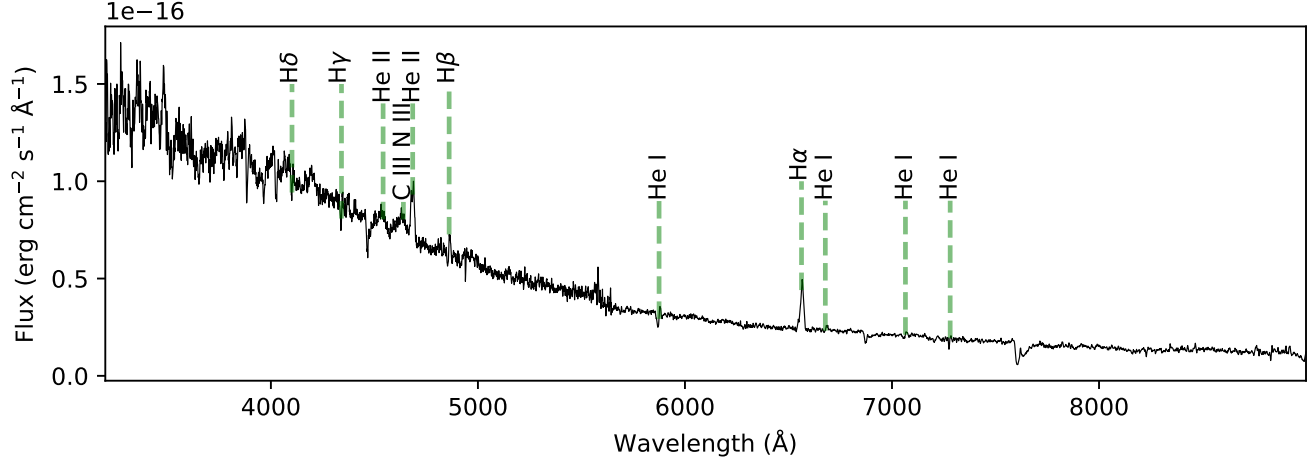


FIG. 5.— The average spectrum of UW CrB taken using the MODS instrument. The most prominent emission lines are marked. The change in the signal to noise ratio at  $\sim 5700$  Å is where the blue detector ends and the red detector begins.

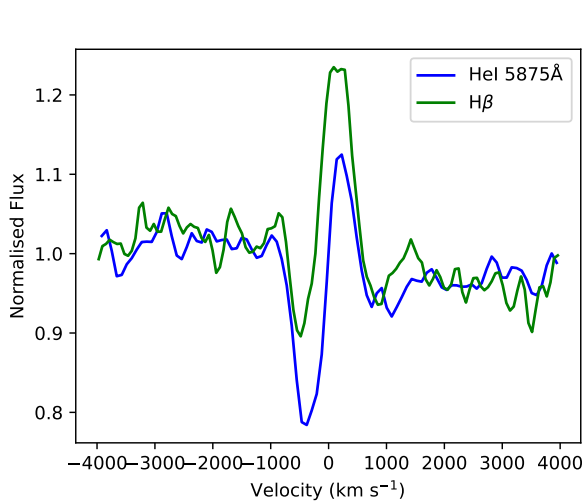


FIG. 6.— The average line profiles of  $H\beta$  (green) and  $He I$  5875 Å (blue), showing strong blue shifted absorption and red shifted emission.

et al. 2013) implemented in PYTHON using PYMULTINEST (Buchner et al. 2014).  $A$  and  $t_0$  were both sampled using flat priors, while a Gaussian prior centered on 20 s with  $\sigma = 10$  s was assumed for  $\tau$ . We additionally fit the 7 bursts originally presented in Mason et al. (2015), since these bursts were never analysed in this way.

Figure 10 shows the results of this fitting when applied to the burst numbered 9 in Figure 1, with the time of this plot being an arbitrary cut in the data around the burst. The start time of the burst is measured to an accuracy 0.38 s based on reproducing the correct flux levels in the first and second bins of the burst, while the  $e$ -folding time is constrained within 2 s (all errors are quoted at the  $1\sigma$  level).

The results of applying this method to all of the 10 bursts observed using GUF1 and the 7 bursts from Mason et al. (2015) can be seen in Figure 11. In this plot, the best-fit  $t_0$  has been subtracted from data such that all of the plots have  $t = 0$  located at the peak of the burst. There is a large scatter in the measured  $e$ -folding times, ranging from  $11 \pm 3$  s at the shortest up to  $32 \pm 3$  s. The

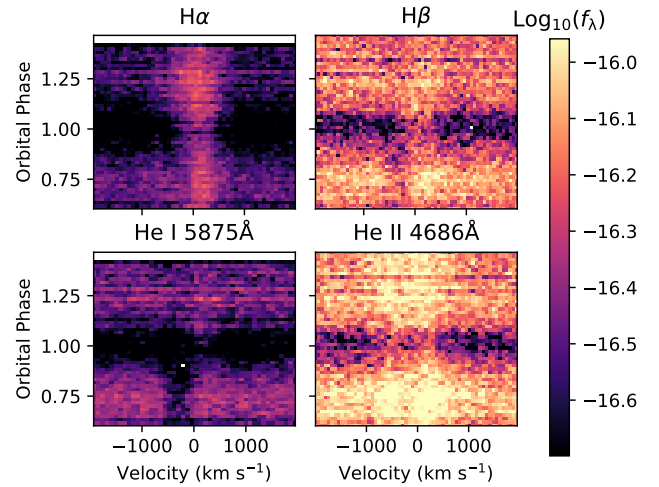


FIG. 7.— The trailed spectra of  $H\alpha$ ,  $H\beta$ ,  $He II$  and  $He I$  (going clockwise from top left). These trailed spectra show how the intensity (represented by the colour) of the lines varies over the orbital phase. In particular, all the lines experience a drop in intensity during eclipse.  $He II$  shows a strong double peaked nature throughout the binary orbit, while  $He I$  shows transient absorption.

observed  $e$ -folding times are in good agreement with the range of values between 15–28 s and 15–27 s reported in Hynes et al. (2004) and Hakala et al. (2009).

### 3.3.2. Modelling the optical bursts II - HiPERCAM

The burst detected using HiPERCAM is shown in Figure 12, and represents a substantial increase in data quality over the rest of the data present in this paper. As such, we attempted to fit this burst with a physically motivated model, as opposed to the simple exponential of Equation 3.

Creating a self-consistent model where an X-ray burst occurs on the surface of the neutron star, then heats the elliptical disc and the exposed surface of the companion star is not feasible with current binary star modelling programs. Given the many unknowns regarding the structure of the accretion disc, and the complexity introduced by its ellipticity, we choose to focus on the companion star, and include a simple model for the ac-

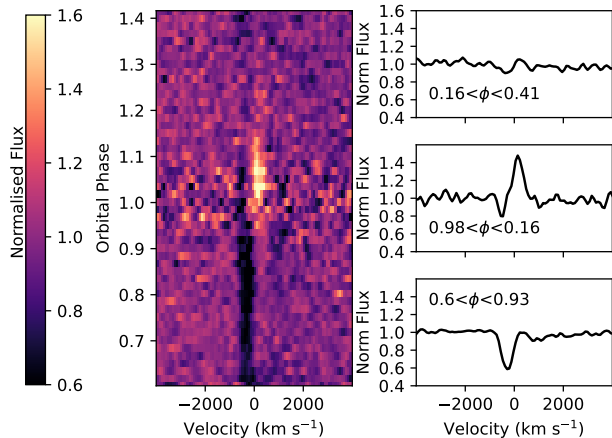


FIG. 8.— The left panel shows the trailed spectrum around Hel 5875 Å. The right panels show the average spectrum for selected orbital phases, highlighting when the line displayed strong absorption, strong emission and just continuum. The spectra here have been smoothed by convolving the spectrum with a gaussian with a  $\sigma = 0.9\text{Å}$ .

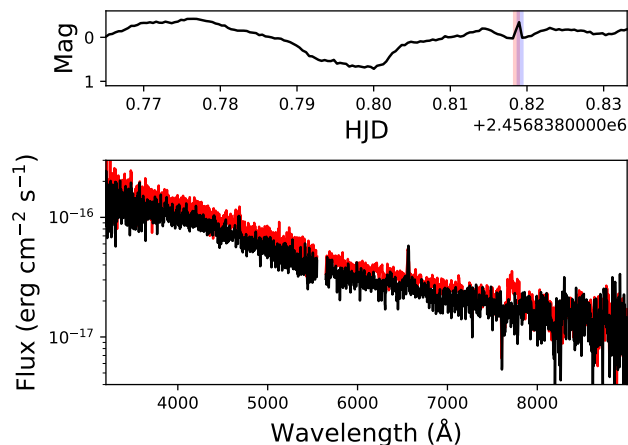


FIG. 9.— The top panel shows the LBC light curve, focused on the time around the optical burst. The transparent red region highlights the time when the red spectrograph of MODS1 was exposed, while the transparent blue region highlights the time when the blue spectrograph was exposed. The main panel shows the entire optical spectrum observed during the burst (red) versus the average of the spectra taken directly before and after the burst (black).

cretion disc.

We used the ICARUS code (Breton et al. 2012) to create a model of the companion star in UW CrB, where irradiation of the companion star is allowed to vary over the duration of the optical burst. There are a few caveats to this model which we outline in the following paragraphs, before discussing our results.

First, in order to generate the companion’s surface, the binary parameters for the system must be specified. As input, ICARUS requires the following: the mass ratio of the binary ( $q = M_{\text{NS}}/M_{\text{Comp}}$ ), the orbital period of the binary ( $P_{\text{O}}$ ), the inclination of the binary,  $i$ , the projected radial velocity amplitude of the companion star ( $K_{\text{Comp}}$ ), the co-rotation factor of the companion ( $\Omega$ ), the Roche-lobe filling factor of the companion ( $f$ ), the exponent of the gravity-darkening law ( $\tau_{\text{grav}}$ ), the base temperature of the companion star ( $T_{\text{base}}$ ), the irradiat-

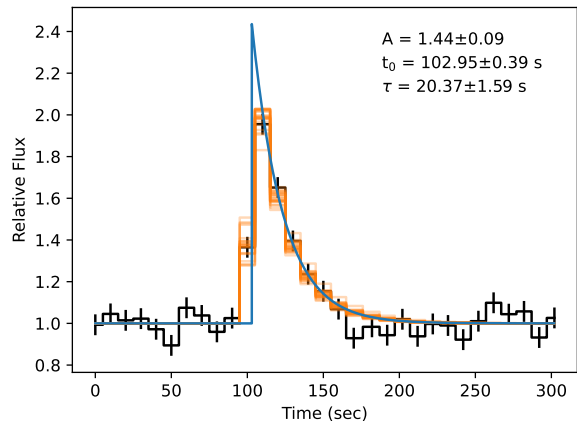


FIG. 10.— The results of fitting Equation 3 to burst 9. The best-fit parameters and errors are given in the top right, and the blue line shows the best-fit model when sampled with a time resolution of 0.01 s. The orange values show 100 models binned to the same temporal resolution as the data (black with associated errors) with parameter values drawn from the posterior distributions.

ing temperature affecting the companion star ( $T_{\text{irr}}$ ), the distance modulus of the binary ( $DM$ ), and the number of magnitudes of extinction in the direction of the binary in the Johnson V band ( $A_V$ ).

Several of these parameters are not constrained for UW CrB, for which we make informed assumptions about in order to reduce the parameter space. First, the neutron star and companion star masses are unknown. As such, we assume a canonical neutron star mass of  $1.55 M_{\odot}$ , and allow the companion mass to vary between 0.1 and  $1.0 M_{\odot}$ , in line with the expected companion mass for a binary with an orbital period of 0.08 days. This leads to a mass ratio of between 1.55 and 15.5 respectively. We assume tidal locking ( $\Omega = 1$ ), and we fix the Roche lobe (RL) filling factor to 1, as we know that RL overflow is feeding the accretion disc. Finally, we fix the orbital period of the binary to 0.077067223 days, in line with the value obtained in this work.

For the accretion disc, we assume it is represented by the summation of a series of annuli, each radiating with a different black body temperature, and that the resultant spectrum is the sum of the contributions from each annulus. Each annulus produces black body radiation with a temperature given by  $T(r) = T_{\text{in}}(r/R_{\text{in}})^{-0.75}$ , where  $T_{\text{in}}$  is the temperature at the most inner part of the disc,  $R_{\text{in}}$ . This parameterisation gives us three parameters to fit: the inner temperature of the accretion disc ( $T_{\text{in}}$ ), the ratio of the inner radius of the accretion disc to the outer radius, and a scaling factor ( $S_g$ ), which we define as the contribution of the disc to the observed  $g'$  flux.

Without any information on the size of the disc, we fix the ratio of the radii to 0.01. Additionally, with no obvious absorption features from the companion star visible in the optical spectrum of UW CrB shown earlier in this paper, we set a lower limit on the scaling parameter of 0.75, meaning that the accretion disc model should account for >75 % of the light at  $g'$  band, with the companion contributing up to 25%.

Assuming this setup, there are two stages to the fitting. The first stage fits the pre-burst light curve in order to constrain the parameters  $T_{\text{base}}$ ,  $T_{\text{irr}}$ ,  $i$ ,  $DM$ ,  $T_{\text{in}}$ ,  $S_g$  and



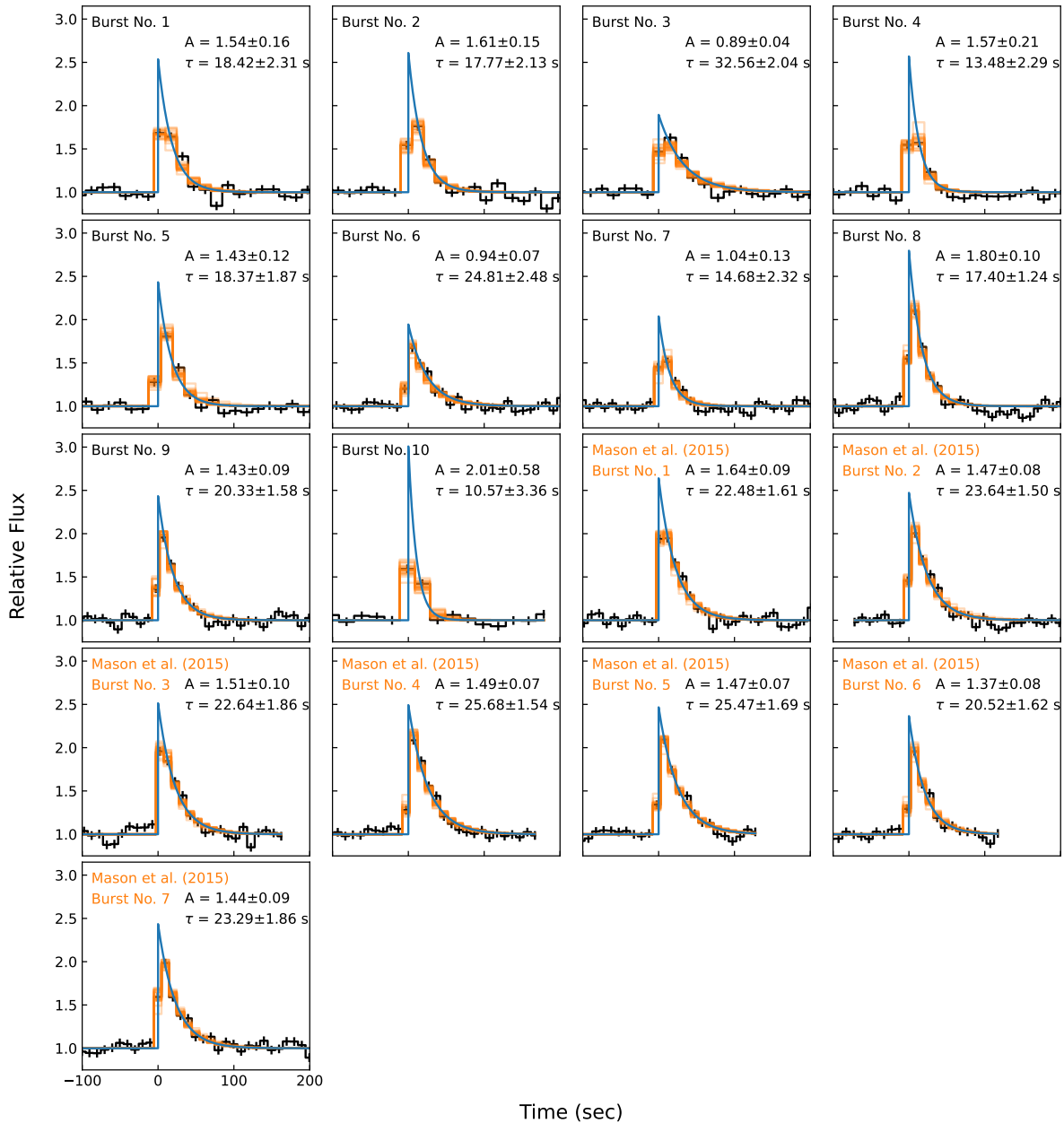


FIG. 11.— The 10 optical bursts observed with the GUFU instrument and 7 from Mason et al. (2015) (in black) along with the resulting model from fitting Equation 3 (blue). The orange lines here represent 100 models drawn from the posterior distributions of the parameters of each burst so as to give an idea of the error in the model. The value of  $t = 0$  corresponds to the peak amplitude in the model burst. The error in the amplitude of Burst 10 is significantly higher than the other bursts due to the longer cadence of these data.

$A_v$ .

In the second stage, all of these parameters were frozen other than  $T_{\text{irr}}$ , and the burst light curve was fit. As such, for each data point of the burst, we calculate the contribution from the companion star assuming the binary parameters which are fit to the pre-burst light curve, and then optimise the irradiating temperature to minimise the difference between the observed flux and the expected contributions of the disc and the star.

The parameter space was explored using EMCEE (Foreman-Mackey et al. 2013), with 32 walkers allowed

to evolve over 50,000 steps, with 1,000 steps were discarded as a burn-in. The corner plot of the resulting parameter space is included in Appendix A. The best fitting parameters are given in Table 3, and the best fitting model shown in Figure 13. There are a few caveats to our results. First, the disc contribution converged to 0.75, the bottom of the prior range. While it may be tempting to lower this limit, the lack of spectral features from the secondary forbids this. Additionally, the temperature of the companion star and the irradiation it is subjected to outside of the burst are likely not physical

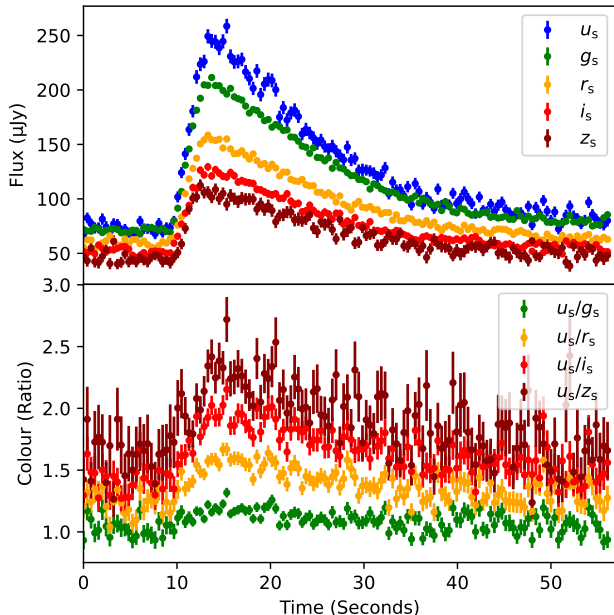


FIG. 12.— The optical burst observed using HiPERCAM in the 5 SDSS bands, plotted in calibrated flux density (top), and as a ratio of the u-band to each separate band (bottom). Here, the absolute time of the first datum has been subtracted off to give clarity to the duration of the burst rise and decay time.

TABLE 3  
BEST FITTING BINARY PARAMETERS FROM THE ICARUS MODELLING OF THE HiPERCAM LIGHT CURVES

Parameter	Value
$T_{\text{base}}$ (K)	$5500^{+700}_{-900}$
$T_{\text{irr}}$ (K)	$9000 \pm 400$
$T_{\text{in}}$ (K)	$(8 \pm 1) \times 10^5$
$i$ ( $^\circ$ )	$70 \pm 10$
DM	$14.0^{0.3}_{-0.5}$
$S_g$	$\zeta 0.75$
$A_v$	$0.58 \pm 0.03$

constraints, as the values presented here assume the orbital variability in the light curve are all arising due to changing viewing aspects of the companion star. This is certainly not true, as the elliptical disc is likely contributing some fraction of the variability, especially if eclipses are occurring. However, while being nonphysical, the model is still useful for understanding the optical bursts. That is, the models show that increasing the temperature of the companion star dramatically can adequately model the burst (at least in most bands).

Figure 14 shows the evolution of the irradiating temperature over the course of the burst. Pre-burst, this value is at 9,300 K, suggesting the companion star is undergoing significant heating. Then, as the burst begins, it quickly rises to 28,000 K, followed by a slow decline. While this model can account for the overall shape of the  $g_s$ ,  $r_s$ ,  $i_s$ , and  $z_s$  (up to a systematic offset which can be ascribed to a small photometric band calibration offset), the same cannot be said of the  $u_s$ . This suggests that the burst spectrum may deviate from a black body at short wavelengths. This could be due to additional components which we are not accounting for, such as irradiation of the disc.

To improve on this model, a simultaneous optical and X-ray burst should be observed, with a time resolution similar to the HiPERCAM data presented here. Such a data set would allow for a lag to be measured, which would directly pinpoint the location of the reprocessing and allow for refinement of this model.

### 3.3.3. Orbital phases of the bursts

The relative fluence of all 17 optical bursts and the phases at which they occurred presented this paper were added to the 33 optical bursts listed in Mason et al. (2012), the 7 first presented in Mason et al. (2015), and the 5 bursts detected with the HST. Figure 15 shows a polar plot of the bursts, with the angle of the burst representing the orbital phase at which the burst occurred, and the radial extent of the burst representing the relative fluence of the burst. For this plot, we have normalised fluences of each burst by the median fluence observed with a given instrument+filter combination. This is to remove wavelength dependencies on the fluence, but we acknowledge it may be biasing the distribution if not enough bursts have been observed such that the observed median is not representative of the underlying, true median of fluences.

The gap in orbital phase during which no bursts had been observed by Mason et al. (2012) now has 4 bursts present in it. Mason et al. (2012) initially proposed that the apparent gap centred around orbital phase 0.967 was due to an eclipse of the reprocessing region, masking the reprocessing site from view. The detection of these two bursts rules out this theory. The four bursts had a relative fluence which was comparable to the average relative fluence of all the bursts, suggesting that the reprocessing sight is not being eclipsed.

## 4. THE ORIGIN OF THE EMISSION AND ABSORPTION FEATURES.

The optical minimum in UW CrB has been interpreted as the partial eclipse of the accretion disc in the system by the secondary star. This constrains the inclination of UW CrB to be close to  $80^\circ$  (Mason et al. 2008). The trailed optical spectra here support such an inclination for the system. HeII has a relatively high ionisation energy, meaning it must be coming from a location within the system which is substantially hotter than the location which produces the lower ionisation emission features of HeI and the Balmer features. Given the double peaked nature of the trailed spectrum, this region is likely to be within the inner part of the accretion disc. The lack of an eclipse in this line (only visible when the spectra are normalised to the continuum, see Figure 16), could suggest that this region of the disc is not blocked at any time by the secondary star.

However, this is not the only configuration which would produce a double peaked HeII line without an eclipse. Within other LMXBs, double peaked emission features have been detected even when the disc continuum has been eclipsed. Such behaviour has been proposed to be due to the origin site of the emission features lying above, but co-rotating with, the accretion disc (Somero et al. 2012). This is perhaps the case in UW CrB - in our spectra, the brightest emission line ( $H\alpha$ ) is never fully eclipsed, and is only slightly reduced in flux during the eclipse. This observed behaviour in other systems means

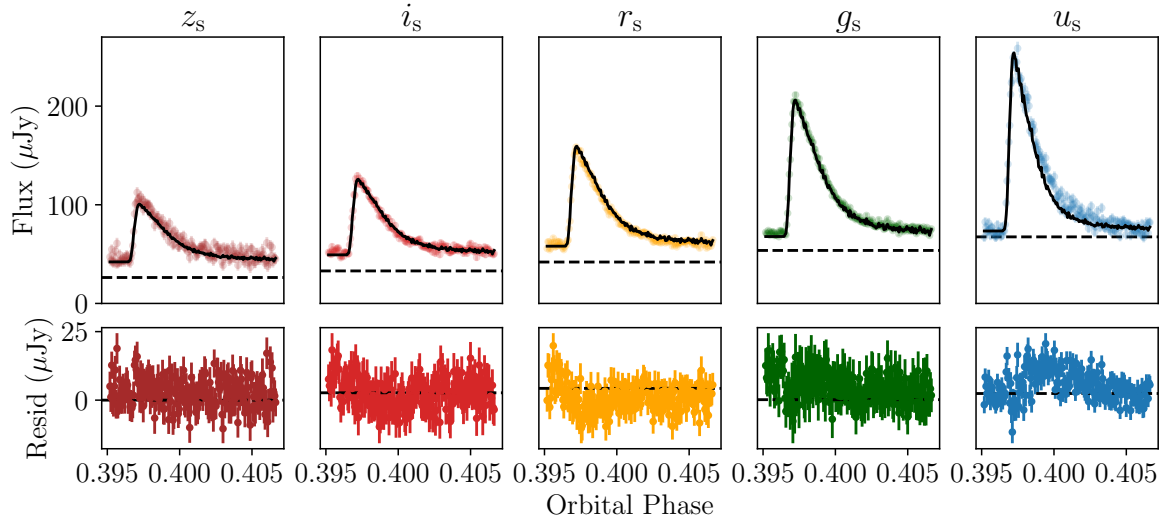


FIG. 13.— Best fitting ICARUS model to the optical burst from UW CrB detected using HiPERCAM. Each panel shows the data from one of the filters (left to right:  $z_s$ ,  $i_s$ ,  $r_s$ ,  $g_s$ ,  $u_s$ ), along with the model as a solid black line. The dashed line shows the constant contribution to each band from the accretion disc.

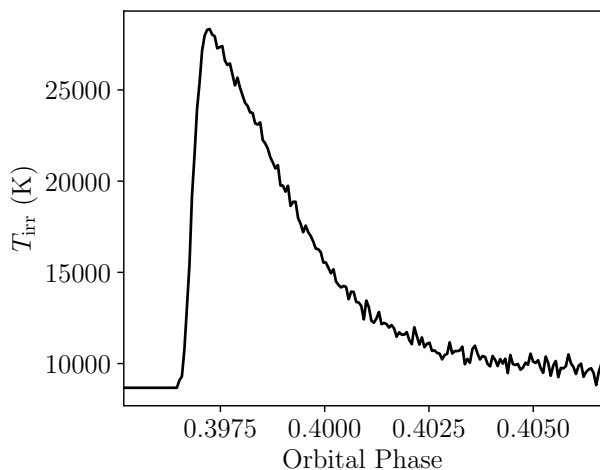


FIG. 14.— Evolution of the irradiating temperature parameter over the course of the burst for the best fitting model, showing that the peak temperature of the optical burst region reaches 28,000 K.

inferring an inclination of  $80^\circ$  based solely on the behaviour of the emission features in the spectra would be unwise.

The behaviour of the HeI and Balmer lines suggest that these features are coming from a region which is in the outer part of the accretion disc. The orbital-phase dependant blue absorption features are consistent with an outflow from the system. Initial evidence for such an outflow has been recently proposed by Fijma et al. (2023), who found a transient, blue shifted absorption feature in far-UV spectra of UW CrB. However, the profiles of the features presented here are slightly different to those presented by Fijma et al. (2023). In the UV data presented in that paper, the emission features extend up to  $-1000 \text{ km s}^{-1}$  with a noticeable absorption dip embedded in the line profile at  $-500 \text{ km s}^{-1}$ , while there is an additional absorption feature at an even higher velocity of  $-1500 \text{ km s}^{-1}$ . In the data presented here, we only see an absorption feature at a velocity of  $-500 \text{ km s}^{-1}$ ,

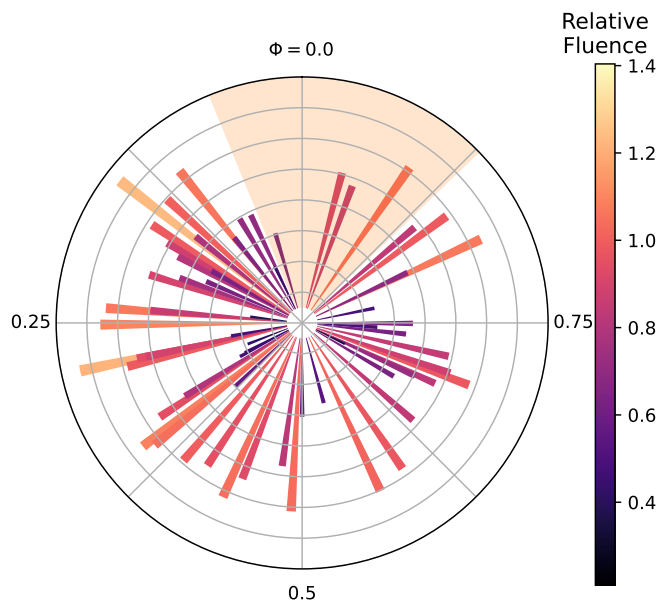


FIG. 15.— The fluences and orbital phases of every optical burst seen in UW CrB. This combines the 17 optical bursts presented in this work, the 4 UV bursts seen with the HST, the 33 optical bursts listed in Mason et al. (2012), and the 7 bursts shown in Mason et al. (2015). The orange shaded region shows the gap identified by Mason et al. (2012). There are now 4 detected bursts in this region.

with no blue shifted emission and no higher velocity absorption feature. It may be that the cause of the  $-500 \text{ km s}^{-1}$  feature in the optical lines is responsible for the same feature in the UV data. However, this is likely not a disc wind, as these tend to cause features at much higher velocities in high-inclination systems ( $> 1000 \text{ km/s}$ ; see e.g. Panizo-Espinar et al. 2022 Table 2, also Cúneo et al. 2023), alike to the high-velocity component identified at UV wavelengths by Fijma et al. (2023).

## 5. CONCLUSIONS

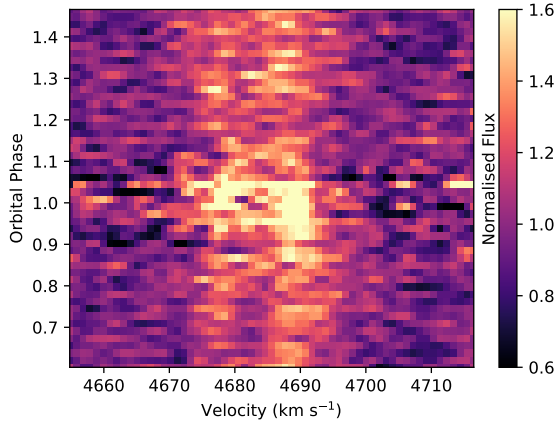


FIG. 16.— Trailed HeII 4686 Å line after normalising to the continuum. These data show that the double peaked line persists throughout the eclipse, meaning it is not blocked by the secondary star.

Four optical bursts have now been observed during the orbital phase gap observed by Mason et al. (2012), suggesting the site of reprocessing is not eclipsed as previously thought. However, it remains to be seen whether the presence of an orbital phase gap depends on the phase of the 5.5 day precessing accretion disc. Since it is possible that the reprocessing site is located within the disc, it is also possible that during certain parts of the 5.5 day precession of the disc, this site does become eclipsed during the orbital phases observed by Mason et al. (2012) (logically, this would be when the site lies in between the NS and the secondary), and that during the other phases of the precessing disc, this site is not eclipsed (logically, this would be when the site lies on the far side of the NS, furthest from the companion). This argument is fully dependant on whether the reprocessing site is in the disc, which is yet to be confirmed. One thing is for certain - further optical monitoring of UW CrB, preferably over the 5.5 day disc period, should be performed to see if the appearance of the bursts is dependant on the phase of the disc.

The optical spectra presented here raise more questions than they answer. Previously, the P Cygni profiles seen in HeI and H $\beta$  were thought to arise due to a wind from the NS. However, our time resolved spectra show that the

blue absorption wing of these lines is transient, which is not expected for a wind component. It may be that our viewing angle of the accretion structures changes through the orbit, which leads to different amounts of absorption in the lines (this may also be related to the 5.5 day disc precession period). Furthermore, the brightest emission line (H $\alpha$ ) is not fully eclipsed, and is only slightly reduced in flux during the eclipse. This suggests the site of H $\alpha$  emission is not fully eclipsed by the secondary, and could mean that some emission is generated above the plane of the disc. Finally, we have seen evidence of the Bowen blend emission in the averaged spectrum. Further optical spectra with a high time resolution should be obtained to fully characterise the transient nature of the absorption in different spectral lines, and to track the Bowen blend emission over a full orbital period in order to constrain the mass of the NS.

Finally, we have applied a simple model of increased irradiation of the companion star to explain the amplitude and colour of the optical burst. While the model is simplistic, and ignores contributions from the accretion disc, it fits the data well, and shows that the luminosity of the burst is consistent with the inner face of the companion star reaching a temperature in excess of 25,000 K.

#### ACKNOWLEDGEMENTS

M.R.K. and R.P.B. acknowledge support from the European Research Council (ERC) under the European Union's Horizon 2020 research and innovation programme (grant agreement No. 715051; Spiders). M.R.K. also acknowledges support from the Royal Society in the form of a Newton International Fellowship (NIF No. NF171019), and the Irish Research Council in the form of a Government of Ireland Postdoctoral Fellowship (GOIPD/2021/670: Invisible Monsters). P.A.M. acknowledges support from Picture Rocks Observatory. I.P. acknowledges support from a Royal Society University Research Fellowship (URF\R1\231496). D.M.S. and T.M.D. acknowledge support from the Spanish *Agencia estatal de investigación* via PID2021-124879NB-I00.

This work made use of ASTROPY (Astropy Collaboration et al. 2013, 2018), CORNER (Foreman-Mackey 2016), EMCEE (Foreman-Mackey et al. 2013), ICARUS (Breton et al. 2012).

#### REFERENCES

- Astropy Collaboration et al., 2013, *A&A*, **558**, A33  
 Astropy Collaboration et al., 2018, *AJ*, **156**, 123  
 Beals C. S., 1929, *MNRAS*, **90**, 202  
 Breton R. P., Rappaport S. A., van Kerkwijk M. H., Carter J. A., 2012, *ApJ*, **748**, 115  
 Buchner J., et al., 2014, *A&A*, **564**, A125  
 Cúneo V. A., et al., 2023, *A&A*, **679**, A85  
 Dhillon V. S., et al., 2021, *MNRAS*, **507**, 350  
 Doi M., et al., 2010, *AJ*, **139**, 1628  
 Feroz F., Hobson M. P., 2008, *MNRAS*, **384**, 449  
 Feroz F., Hobson M. P., Bridges M., 2009, *MNRAS*, **398**, 1601  
 Feroz F., Hobson M. P., Cameron E., Pettitt A. N., 2013, arXiv e-prints, p. arXiv:1306.2144  
 Fijma S., Castro Segura N., Degenaar N., Knigge C., Higginbottom N., Hernández Santisteban J. V., Maccarone T. J., 2023, *MNRAS*, **526**, L149  
 Foreman-Mackey D., 2016, *The Journal of Open Source Software*, **1**, 24  
 Foreman-Mackey D., Hogg D. W., Lang D., Goodman J., 2013, *PASP*, **125**, 306  
 Giallongo E., et al., 2008, *A&A*, **482**, 349  
 Green J. C., et al., 2012, *ApJ*, **744**, 60  
 Grindlay J. E., McClintock J. E., Canizares C. R., Cominsky L., Li F. K., Lewin W. H. G., van Paradijs J., 1978, *Nature*, **274**, 567  
 Hakala P. J., Chaytor D. H., Vilhu O., Piirola V., Morris S. L., Muhli P., 1998, *Astronomy & Astrophysics*, **333**, 540  
 Hakala P., Hjalmarsson L., Hannikainen D. C., Muhli P., 2009, *Monthly Notices of the Royal Astronomical Society*, **394**, 892  
 Harding L. K., Hallinan G., Boyle R. P., Golden A., Singh N., Sheehan B., Zavala R. T., Butler R. F., 2013, *ApJ*, **779**, 101  
 Homer L., Charles P. A., O'Donoghue D., 1998, *Monthly Notices of the Royal Astronomical Society*, **298**, 497  
 Hynes R. I., Robinson E. L., Jeffery E., 2004, *The Astrophysical Journal*, **608**, L101  
 Mason P. A., Robinson E. L., Gray C. L., Hynes R. I., 2008, *The Astrophysical Journal*, **685**, 428

- Mason P. A., Robinson E. L., Bayless A. J., Hakala P. J., 2012, *The Astronomical Journal*, **144**, 108
- Mason P. A., Robinson E. L., Gomez S., Segura J. V., 2015, *Acta Polytechnica CTU Proceedings*, **2**, 50
- Morris S. L., Liebert J., Stocke J. T., Gioia I. M., Schild R. E., Wolter A., 1990, *The Astrophysical Journal*, **365**, 686
- Muñoz-Darias T., et al., 2016, *Nature*, **534**, 75
- Muñoz-Darias T., et al., 2019, *ApJ*, **879**, L4
- Muhli P., Hakala P. J., Hjalmarsdotter L., Hannikainen D. C., Schultz J., 2004, in *Tovmassian G., Sion E., eds, Revista Mexicana de Astronomia y Astrofisica Conference Series Vol. 20*, *Revista Mexicana de Astronomia y Astrofisica Conference Series*. pp 211–211
- Mukai K., Smale A. P., Stahle C. K., Schlegel E. M., Wijnands R., 2001, *The Astrophysical Journal*, **561**, 938
- Panizo-Espinar G., et al., 2022, *A&A*, **664**, A100
- Parikh A., José J., Sala G., Iliadis C., 2013, *Progress in Particle and Nuclear Physics*, **69**, 225
- Pogge R. W., et al., 2010, in *Society of Photo-Optical Instrumentation Engineers (SPIE) Conference Series*. p. 77350A
- Robinson E. L., Young P., 1997, *The Astrophysical Journal*, **491**, L89
- Schoembs R., Zoeschinger G., 1990, *Astronomy & Astrophysics*, **227**, 105
- Somero A., Hakala P., Muhli P., Charles P., Vilhu O., 2012, *A&A*, **539**, A111

## APPENDIX



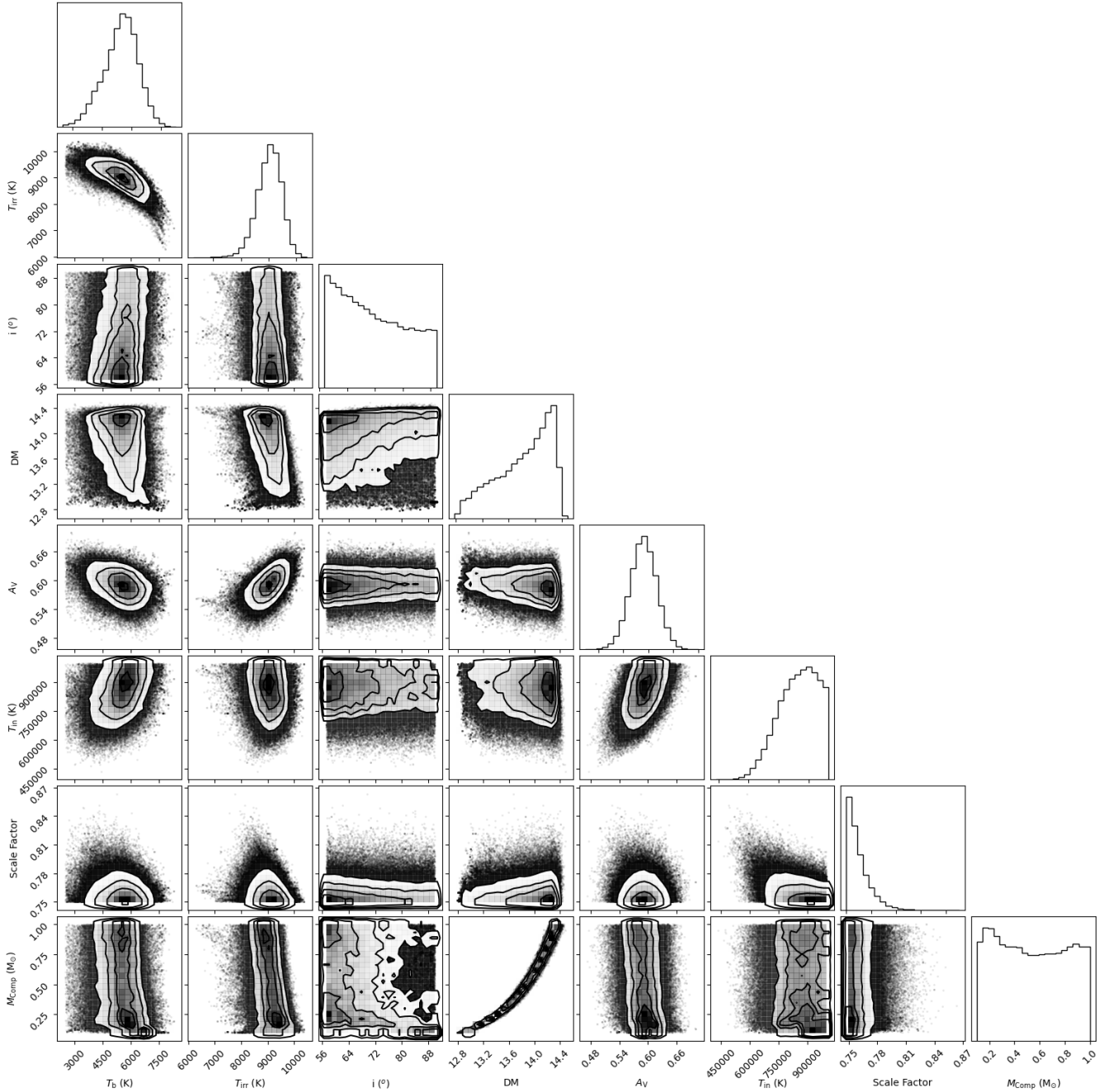


FIG. 17.— Corner plot from the MCMC analysis of the burst observed using HiPERCAM.

#### CORNER PLOTS

This paper was built using the Open Journal of Astrophysics  $\text{\LaTeX}$  template. The OJA is a journal which provides fast and easy peer review for new papers in the **astro-ph** section of the arXiv, making the reviewing process simpler for authors and referees alike. Learn more at <http://astro.theoj.org>.